Colloidal Fe^{III}, Mn^{III}, Co^{III} and Cu^{II} hydroxides stabilized by starch as catalysts of water oxidation reaction with one electron oxidant $Ru(bpy)_3^{3+}$

Andrei S. Chikunov,[a] Oxana P. Taran,[a, b, c] Inna A. Pyshnaya, [d] Valentin N. Parmon [a]

Abstract: Colloidal catalysts for oxidation of water to dioxygen, which are stable on storage and under the reaction conditions, are synthesized based on Co^{III}, Mn^{III}, Fe^{III} and Cu^{II} hydroxides. Stabilization of the colloids with dextrated starch allows the process of hydroxide ageing to be stopped at the stage of the formation of primary nuclei (ca. 2–3 nm from TEM data). Molecular mechanics and DLS studies indicate the core-shell type structure of the catalysts, where the hydroxide core is stabilized by the molecular starch network (ca. 5–7 nm). The colloidal catalysts are highly efficient to oxidation of water with one electron oxidant $Ru(bpy)_3^{3+}$ at pH 7 to 10. The influence of pH, catalyst concentration and buffer nature on the oxygen yield is studied. The maximal yields are 72, 53 and 78 % over Fe-, Mn- and Co-containing catalysts, respectively, and TON are 7.8; 54 and 360, respectively. The Cu-containing catalyst is poorly effective to the water oxidation (the maximal yield is 28 % O_2). The synthesized catalysts are of interest for stopped-flow kinetic studies of the mechanism of the water oxidation and as precursors for anchoring nanosize hydroxides onto various supports in order to develop biomimetic systems for artificial photosynthesis.

Introduction

In the last decade, there is an evident resurgence of interest in the development of photocatalytic systems for water decomposition to hydrogen and oxygen, as well as growing number of publications in the field[1]. The reason is the human demands on alternative energy sources capable of neutralizing the environmental hazards caused by the use of traditional fossil energy resources. Numerous approaches are used for the conversion of visiblelight solar radiation into habitual energy forms (heat and electric energy or chemical interaction energy). But of most interest are the systems for overall photodecomposition of water to molecular oxygen and hydrogen, the so-called artificial photosynthesis systems:

$$2H_2O \xrightarrow{h\nu} O_2\uparrow + 2H_2\uparrow. \quad (1)$$

Application of these systems will allow extra energy loss to be avoided and the energy of light quanta to be stored directly as chemical energy in the hydrogen molecule. The obtained hydrogen can be transported and/or used for generation of the required type of energy. In the implementation of the artificial photosynthesis, the bottleneck is the stage of water oxidation, which required simultaneous transfer of four electrons and four protons from two water molecules[2,3]:

$$2H_2O \xrightarrow{h\nu} O_2\uparrow + 4H^+ + 4e^- \quad (2)$$

Hence, the catalyst for this stage must provide localized accumulation of a considerable oxidation potential[4]. From literature, partially hydrolyzed oxides of some first-transitionrow metals (Mn, Fe, Co, Ni, Cu), as well as Ru and Ir[5-11] are capable of catalyzing water oxidation to molecular oxygen. Thus, we can formulate a number of requirements for the effective catalyst for this process based on general structural features of the said systems and on the structure of the natural oxygen-evolving complex of photosystem II[12]. First, the functional active center of the compounds should be of the hydroxide nature (i.e. the active center is hydroxide (M-OH-M-OH) or partially hydrolyzed oxide (M-O-M-OH) on the surface of catalyst nanoparticle with the external group replaced by -OH)[13] and comprise atoms of the metal capable of having at least three successive oxidation states (for example, these are II, III and IV for Mn, Fe and Co, III, IV and V for Ru, I, II and III for Cu)[14]. Second, the active center of the catalyst should bear free coordination sites or highly labile ligands that are easy to replace by water or OH groups[15] . Third, the ligands used for stabilizing the active center should not be strong electron donors or acceptors. If the ligand is a strong electron donor, then the ligand but not water molecule is preferably oxidized. On the other hand, if ligand is a strong electron acceptor, the electron density over the metal atoms decreases to cause a decrease in the oxidation potential of the catalyst along with a decrease in the acidity of the coordinated OH-group or water molecule[14]. Fourth, the compounds should be capable of forming di- and polynuclear structures of the μ-hydroxo or μ-oxo type[14, 15]. However, the mechanism of action of both natural oxygen-evolving complex and the known compounds capable of catalyzing water oxidation remains an issue for discussion[16-18]. Therefore, the effective catalysts are still selected empirically. There are several approaches –

[a] A.S. Chikunov, Prof. O.P. Taran, Prof. V.N. Parmon
Boreskov Institute of Catalysis (BIC SB RAS)
630090, Novosibirsk, Lavrentieva ave. 5 (Russian Federation)
E-mail: chikunov@catalysis.ru
[b] Prof. O.P. Taran,
Institute of Chemistry and Chemical Technilogy SB RAS (ICCT SB RAS)
660036, Krasnoyarsk, Akademgorodok st. 50-24 (Russian Federation)
taran.op@icct.krasn.ru
[c] Prof. O.P. Taran,
Siberian Federal University
660041, Krasnoyarsk, Svobodny ave. 79 (Russian Federation)
[d] Ph.D. I.A. Pyshnaya,
Institute of Chemical Biology and Fundamental Medicine SB RAS (ICBFM SB RAS)
630090, Novosibirsk, Lavrentieva ave. 8 (Russian Federation)

electrochemical, chemical and photochemical – to implement and/or to investigate the process of water oxidation[19, 20]. Each of these methods has their own advantages and drawbacks. The electrochemical method allows the necessary concentration of electron vacancies to be easily generated in the catalyst. At the same time, the evolution of the catalyst surface can be in situ monitored using electrochemical and spectroscopic techniques. Nevertheless, there are some drawbacks such as the necessity to organize the electron transfer from the supporting electrode to the catalyst and impossibility of identifying individual stages of successive accumulation of oxidation equivalents by the catalyst active center. The application of one-electron oxidants prepared either chemically or photochemically makes it possible to identify elementary steps of oxidation of the active center. Unfortunately, chemical oxidants can provoke some side processes, e.g. destruction of organic ligands in the oxidant and/or catalyst. In addition, considerably different behaviors may be characteristic of identical catalysts when different method for the oxidant generation and reaction conditions are used[21]. There are also same other factors which make it difficult to study the mechanism of the water oxidation. First, the rate of the four electron oxidation of water is extremely high: the time of releasing molecular oxygen is ca. 1 ms[22]. Second, hydroxo compounds of the mentioned metals are unstable under weak alkaline conditions, which are optimal for the artificial photosynthesis. They tend to coagulate and to form a bulky hydroxide phase at pH higher than 7.0 [23]. This undesirable growth of the hydroxide particles may be prevented using stabilizing ligand molecules[24]. However, there are numerous additional requirements on the nature of ligands to be used at strong oxidative conditions of the reaction. The ligands must provide water solubility of the catalyst complex, feature a moderate donor or acceptor properties (otherwise, the ligand will be preferably oxidized rather than water molecule, or overpotential of water oxidation will increase substantially due to a redistribution of the electron density on metal ions), be easily hydrolysable or have unoccupied coordination sites to make the catalyst active site accessible for the oxidant and substrate molecules[15]. A successful example of this approach was suggested earlier[25, 26]. The proposed method is to stabilize the transition metal hydroxide in water solutions via addition of natural glucose biopolymer – molecular starch. Colloidal hydroxides of manganese[25] and cobalt[26] allowed high oxygen yields (up to 65 and 85 % in respect to the reaction 2 stoichiometry, respectively) to be obtained through water oxidation by tris-bipyridyl complex of trivalent ruthenium $Ru(bpy)_3(ClO_4)_3$. In the present study we prepared colloidal catalysts based on starch stabilized hydroxides of Fe^{III} and Cu^{II} and compared them with the catalysts based on Mn^{III} and Co^{III} for water oxidation with $Ru(bpy)_3(ClO_4)_3$ complex. We also studied for the first time the structures of the starch stabilized colloidal hydroxides using a set of physicochemical techniques (photon correlation light scattering and transmission electron spectroscopy) and computational method of molecular mechanics. The obtained results allowed us to understand the reasons for the high efficiency of colloidal catalysts for water oxidation reaction.

Results and Discussion

The procedure for the catalyst preparation was optimized by varying the following parameters: 1) the sequence of mixing the reactants (catalyst precursor and alkali); 2) the reaction temperature; 3) pH; 4) the concentration and properties of the starch stabilizer.

Table 1. Oxygen yields in the presence of Mn-, Fe-, Co- and Cu-contained catalysts prepared with various techniques. $[Ru(bpy)_3^{3+}] = 5\times10^{-4}$ M, 0.06 M borate buf., pH=9.2, 298 K.

Entry	Active component [conc., M]	Starch, [wt. %]	Synthesis technique	*T*, [K]	pH	Aging period, [h]	$S(O_2)$, [% stoich.]
1	Co (5×10^{-5})	1.25	1 [c]	350	11.0	24	60
2		1.25	2 [c]	350	11.0	24	54
3		1.25	3 [c]	350	11.0	24	66
4		1.25	3 [c]	298	11.0	24	50
5	Mn (10^{-5})	1.25	3 [c]	298	11.0	24	25
6		1.25	3 [c]	350	11.0	24	46
7		1.25	3 [c]	350	11.0	168	41
8		0.75	3 [c]	350	11.0	24	48
9		0.75	3 [c]	350	11.0	168	37
10		0.125	3 [c]	350	11.0	24	52
11		0.125	3 [c]	350	11.0	168	-
12	Cu (5×10^{-5})	1.25	3 [c]	350	11.0	24	7
13		1.25	3 [c]	298	11.0	24	25
14		1.25	3 [c]	298	7.0	24	19
15		1.25	3 [c]	298	5.0	24	16
16	Fe (10^{-6})	1.25	3 [c]	350	11.0	24	64
17		1.25	3 [c]	350	11.0	168	51
18		0.625	3 [c]	350	11.0	24	65
19		0.625	3 [c]	350	11.0	168	57
20		0.125	3 [c]	350	11.0	24	66
21		0.125	3 [c]	350	11.0	168	65

[a] Addition of Co solution to the solution of starch and NaOH, [b] Addition of NaOH solution to starch and Co solution, [c] Addition of small portions of Co and NaOH solutions alternately to the solution of starch.

We studied the influence of the mixing sequence on the yield of O_2 with Co-containing catalyst as an example. We used three methods for the reactant mixing: (1) 1M NaOH (to achieve pH

11.0) was added to the aqueous solution of starch and Co-precursor; (2) the Co-precursor was added to the aqueous starch solution with pH 11.0 (350 K); pH was elevated down to 6.7 than 1M NaOH was added to reach pH 11.0; (3) dropwise addition of the Co-precursor and small portions of alkali (1M NaOH) were added alternately to the aqueous starch solution at pH kept constant (11.0). (Table 1, Nos. 1–3). The prepared catalysts were tested for water oxidation with tris-bipyridyl complex of trivalent ruthenium:

$$4Ru(bpy)_3^{3+} + 2H_2O \rightarrow 4Ru(bpy)_3^{2+} + 4H^+ + O_2\uparrow \quad (3)$$

The catalyst prepared by method 3 provided a higher yield of O_2 (65 %) than the catalysts prepared by methods 1 and 2 (60 and 54 % of the stoichiometric yield, respectively). The results obtained can be understood based on the data reported by H. Zhang et al.[27] who used the method of molecular dynamics for studying the process of the formation of primary particles of hydroxo compounds. The author established that disordered 1–2 nm hydroxide clusters are only formed at low concentrations of the hydrolyzed salts. Furthermore, in situ analyses (SAXS, Cryo-TEM, UV-Vis and light scattering) of Fe^{III} hydroxide nucleation process showed that the primary nuclei are formed at the initial stages of hydrolysis as small spherical species[28, 29], 1 to 2 nm, sometimes up to 7 nm in diameter. In the case under consideration, only third method allowed hydrolysis of small concentration of the precursor because each added portion of the cobalt complex solution provided the cobalt concentration equal to 10^{-4} M in the presence of excess starch in the solution. The pH was kept constant (11.0) that led to deprotonation of most of hydroxyl groups of starch due to the right shift of equilibrium:

$$\cdots C\text{-}O^- + H_2O\text{-}Co^{3+}\cdots \square \cdots C\text{-}O\text{-}Co^{2+}\cdots + H_2O \quad (4).$$

As a result, each successive portion of the metal-containing precursors was hydrolyzed to form nanosize primary hydroxide particles[30] and stabilized with the starch polymer that prevented the further growth of the hydroxide particles. Method 1 also implies the formation of the catalytically active low polymerized hydroxo compounds at the early stage of hydrolysis (with the minor quantity of added Co), but the reaction mixture is substantially acidified during the reaction. This change in pH (decrease down to pH 6.0) causes a decrease in the number of deprotonated starch groups and inhibit the hydroxide to starch binding that leads to deeper coagulation of the hydroxide particles. Again, hydrolysis by method 2 produces the least selective catalyst due to weak bonding of hydroxide particles with starch because of the insufficient concentration of OH^-. Similar results were obtained elsewhere[26]. The optical absorption spectrum of the Co-containing catalysts hydrolyzed in excess of starch was characteristic of the initial hydrolysis products. Coarser hydroxide particles were formed with a smaller quantity of starch to shift the absorption bands towards the long-wave region. The temperature of the catalyst preparation influences considerably the catalytic properties. Co-, Mn-, Cu-containing catalysts (Table 1, Nos. 4, 5, 13 and 3, 6, 12) were used for studying the influence at T= 298 and 350 K. Co- and Mn-containing catalysts prepared at 350 K (Nos. 3 and 6) provided much higher yields of oxygen (66 and 46 %, respectively) than similar catalysts prepared at low temperature (50 and 25 %, Nos. 4 and 5 respectively). Evidently, hydrolysis at high temperature resulted in shifting of equilibrium 4 to the right. In addition, higher efficiencies of the catalysts prepared at 350 K indicates the acceleration of bonding of the formed hydroxide particles with starch at the elevated temperature rather than the hydroxide nucleation. On the contrary, with the Cu-containing catalyst, the yields of oxygen decreased from 25 to 7 % over catalysts Nos. 13 and 12 synthesized at 350 and 298 K, respectively. The reason is the reduction of Cu^{II} to Cu^{I} owing to the interaction with the aldehyde group of starch[31] at elevated temperature, the solution is clouding and change its color from blue to yellow. The influence of pH of hydrolysis was studied with the Cu-containing catalyst (Table 1, Nos. 13, 14, 15). Copper hydroxide is more soluble (SP = 2.2×10^{-20}) than that of Fe^{III} and Co^{III} (3.8×10^{-38} and 1.6×10^{-44}, respectively). We failed to find literature data on the solubility product of Mn^{III} hydroxide. The required pH of the solution for precipitation of copper hydroxide is 5.5 at the used concentration of copper acetate (2×10^{-3} M), and those of Fe^{III} and Co^{III} are 2.4 and 2.3, respectively. Hence, the colloidal Cu^{II} hydroxide is more sensitive to pH and most soluble among the metal hydroxides under study. The oxygen yield over the Cu-containing catalyst increased from 16 to 19 % as pH grew from 5.0 to 7.0 for the catalyst preparation and up to 25 % upon the further growth to pH 11.0. It seems like the shift of equilibrium 4 to the right caused by increasing pH results in an increase in the hydroxyl nuclei bounding efficiency. Note that the formation of the insoluble copper precipitate was expected in the absence of the stabilizer at pH 7.0 and 11.0 but the bulky phase was not formed in the system under consideration. Thereafter, all the catalysts were prepared at pH 11. The studies of the influence of the starch state and concentration on catalytic behavior of the Co-containing catalysts[24] revealed that the best catalytic properties and stability was characteristic of the catalyst stabilized by thermo treated (at 453 K for 8 h) 0.5 % starch, while the stability and catalytic properties were worsened at lower concentrations. We studied the influence of different concentrations (0.125– 1.25 wt %) of thermo treated starch on the properties of Fe- and Mn-containing catalysts. Both fresh catalysts and the catalysts stored for 168 hours were tested for water oxidation (Table 1, Nos. 6, 8, 10 and 7, 9, 11 for Mn; Nos. 16, 18, 20 and 17, 19, 21 for Fe). Fresh samples with the lowest starch concentrations (0.75 wt % starch for Mn, 0.125 wt % starch for Fe) gave the maximal oxygen yields (66 and 52 %, respectively). The Mn-containing catalyst stabilized with 0.125 % starch appeared instable: the formation of insoluble Mn_2O_3 precipitate was observed on ageing of this Mn catalyst. The oxygen yields were lower (48 and 46 %) with the Mn catalysts stabilized by 0.75 and 1.25 % starch, respectively, and decreased further (37 and 41 %) upon the catalyst ageing. The fresh Fe-containing catalyst stabilized by 0.125 % starch provided much higher oxygen yield than the catalysts with 0.65

Table 2. Characteristics of catalysts established by Dynamical Light Scattering (mean size of colloid particle) and Transmittance Electron Microscopy (mean size, interplanar distance and phase). [Fe] = [Mn] = [Co] = [Cu] = 2×10^{-3} M, [Starch] = [Starch N.A.[a]] = 12.5 g L^{-1}.

Sample	DLS		TEM			
	<d> [nm]		<d> [nm]		Interplanar distance [Å] (h k l)	Phase
	24 [h]	168 [h]	24 [h]	168 [h]		
Starch	6± 2	7 ± 3	n.i.[b]	n.i.[b]	n.i.[b]	n.i.[b]
Starch N.A. [a]	17±5	n.i.[b]	n.i.[b]	n.i.[b]	n.i.[b]	n.i.[b]
Fe/ 0.125 % Starch	7 ± 3	64±5	1.9±0.4	2.1±0.3	2.3 (3 2 0)	γ-Fe_2O_3
Fe/0.125% Starch N.A. [a]	14±5	17 ± 5	2.0±0.3	n.i.	2.5 (3 1 1)	Fe_3O_4
Mn/ 1.25% Starch	7 ± 2	n.i.	2.4 ± 0.4	n.i.	3.0 (1 1 2) 2.7 (1 0 3) 2.5 (2 1 1)	Mn_3O_4
Co/ 1.25% Starch	5 ± 2	62±2	2.0± 0.4	2.3±0.5	2.9 (2 2 0) 2.4 (3 1 1)	Co_3O_4
Cu/ 1.25% Starch	68±4	n.i.	~100	n.i.[b]	2.4 (1 1 1) 2.1 (2 0 0)	Cu_2O
			20÷40	n.i.[b]	2.5 (0 0 2) (-1 1 1) 2.3 (1 1 1)	CuO

[a] The starch was not activated, [b] n.i.- not identified.

and 1.25 wt % starch. The 0.125 wt % starch Fe-catalysts preserves high selectivity for at least one week storage (66 % O_2 with the fresh catalyst and 65 % for the stored one). Hence, the starch concentration should be chosen depending on the metal nature. The stronger interaction between the metal and hydroxyl groups of starch, the lower starch concentration is required for preparation of stable and selective catalysts. Excess of starch causes a decrease in the oxygen yield, probably due to blockage of the active center. Thus, high-active colloidal hydroxide catalysts can be prepared by alternate addition of small portions of the precursor and alkali to the aqueous starch solution at 350 K and pH 11, well as by using the minimal quantity of dextrated starch that is sufficient for keeping the catalyst in the colloidal state.

Catalyst characterization

The length of the carbohydrate chain of the not activated and dextrated starch were estimated based on the copper ratio determined using Fehling's solution[31]. The reaction goes through reduction of Cu^{II} ions to Cu^{I} with the aldehyde group of starch. While each starch molecule contains only one aldehyde group, the number of monomers in the polymer can be calculated by formula:

$$n = m(\text{Starch}) \times M(Cu_2O) / m(Cu_2O) \times M(C_6H_{12}O_6) \qquad (5)$$

where n is the number of monomer units of glucose; m(starch) the mass of starch sample, g; $M(Cu_2O)$ molar mass of copper oxide, g mol^{-1} ; $m(Cu_2O)$ mass of the formed copper oxide, g; $M(C_6H_{12}O_6)$ molar mass of the glucose monomer. Thus, the average polymerization degree of 53.1 has appeared to be characteristic of the not thermo treated starch (copper ratio 1.66 ± 0.01), while that equals to 15.4 has appeared to be characteristic of the thermally dextrated starch with the copper ratio of 5.72 ± 0.01. The most efficient catalysts (fresh Fe/0.125%Starch, Mn/1.25%Starch, Co/1.25%Starch, Cu/1.25%Starch, as well as Fe/0.125%Starch 168h, Co/1.25%Starch 168h stored for a week) were characterized using transmission electron microscopy (Figs. 1–3).

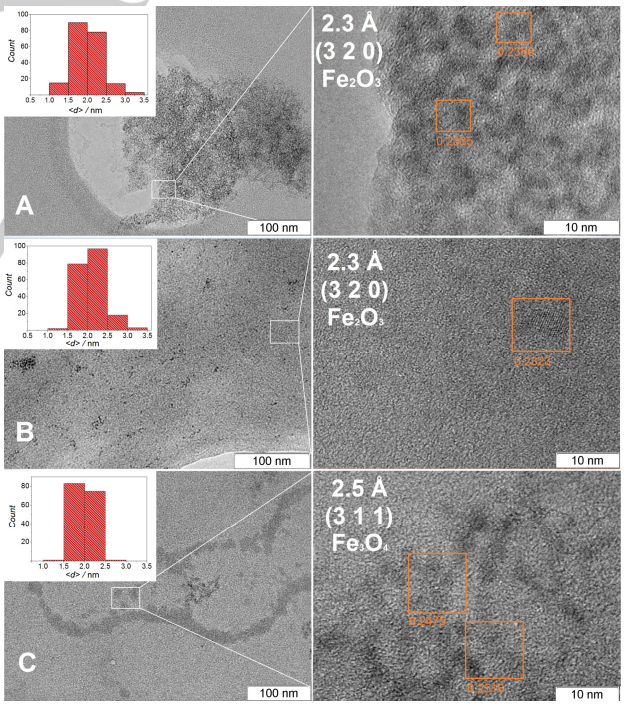

Figure 1. TEM images and particle size distribution for freshly prepared Fe/0.125%Starch catalyst (A), the same catalyst aged during 168 h (B) and catalyst prepared using not activated starch (C). [Fe]= 2×10^{-3} M, [Starch] = [Starch N.A.] = 1.25 g L^{-1}

TEM images of Mn-, Fe-, Co-containing catalysts demonstrate round-shape particles confined in a structured carbohydrate matrix. The observed interplanar distances of 2.3; 3.0, 2.7, 2.5; 2.9, 2.4; 2.4, 2.1 и 2.5, 2.3 Å relate to the following oxides: Fe_2O_3, Mn_3O_4, Co_3O_4 and CuO, respectively (Table 2). Apparently, the oxides are formed under the action of the microscope electron beam as a result of removal of water and hydroxyl groups from the specimen structure. In the image of the aged Co/1.25%Starch 168h catalyst (Fig. 2B(1)), disperse colloidal particles of cobalt oxide (Co_3O_4) are observed along with coarse crystallites (up to 100 nm in length, up to 30 nm in width) with the morphology characteristic of cobalt hydroxide.

However, interatomic distances observed in these crystallites (Fig. 2C, electron diffraction pattern of range B1) equal to 2.9 and 2.4 Å are related to reflections (220) and (302) of cobalt oxide (Co_3O_4). The observed preservation of crystallite morphology identical to cobalt hydroxide indicate very mild conditions of the catalyst reduction during the TEM characterization. The average size of the particles was statistically calculated for the Co/1.25%Starch, Fe/0.125%Starch and Mn/1.25%Starch catalysts (Table 2, histograms in Figs. 1 (A, B, C), 2 (A, B) and 3 (A). In the fresh Fe-containing catalyst, the colloidal particles are 2.0 ± 0.4 nm in size, they practically do not change on storage for a week (2.1 ± 0.3 nm). In the images, there are small amounts of 5 to 50 nm agglomerates of Fe_2O_3 particles formed, probably, after.

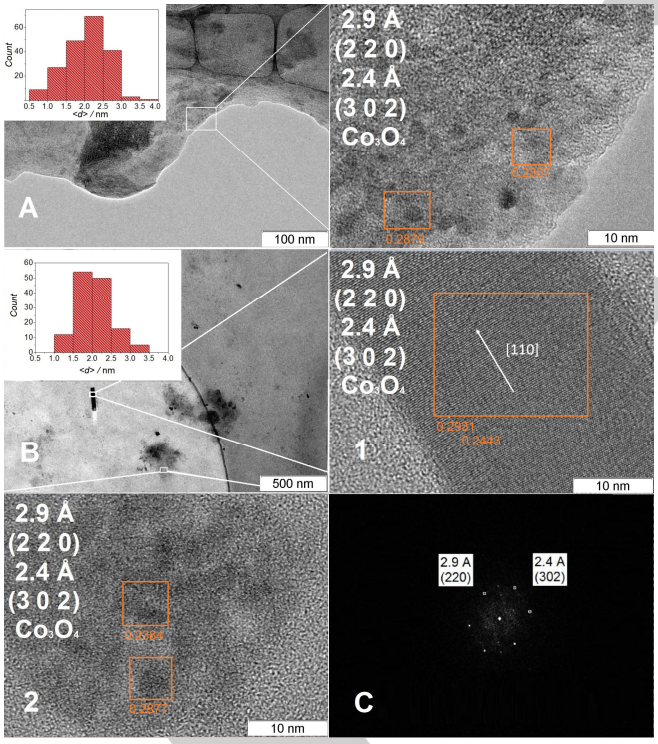

Figure 2. TEM images for Co/1.25%Starch catalysts: freshly prepared (A) and aged during 168 h (B). Inserts: Co3O4 crystal with morphology of hydroxide CoOOH (B1), electron diffraction (C) of area B1, colloidal nanoparticles of Co catalyst (B2). [Co] = 2×10^{-3} M, [Starch] = 12.5 g L^{-1}.

The Fe-containing catalyst stabilized by non-activated starch contains larger particles (2.2 ± 0.3 nm) (Fig. 1C). In the images, there are also observed agglomerates of Fe_3O_4 particles with interplanar distance of 2.5 Å characteristic of reflection (311). These agglomerates are clearly seen to reside on the outer surface of the carbon matrix formed from starch molecules. In the fresh Co-containing catalyst (Fig. 2A), the colloidal particles are 2.0 ± 0.4 nm in average size (Table 2) and grow negligibly in size on storage (Fig. 2B). However, the aged sample comprises a noticeable quantity of 15 to 100 nm agglomerates of Co_3O_4 crystallizes. Images of the fresh Mn-containing catalyst demonstrate disperse Mn_3O_4 particles (3.2 ± 0.4 in size, see Fig. 3A) but not coarse crystallites. Coarse lamellar crystallites of Cu_2O (10 to 100 nm, see Fig. 3B1) are seen in images of the Cu-containing catalyst. Particles of CuO of 20 nm in average diameter also are observed to form agglomerates of several hundred nm of size (Fig. 3B2). The copper catalyst solution is transparent and blue colored. Hence, the predomination of one-valent copper observed in the images can be accounted for by hydroxide reduction under the action of electron beam of the microscope.

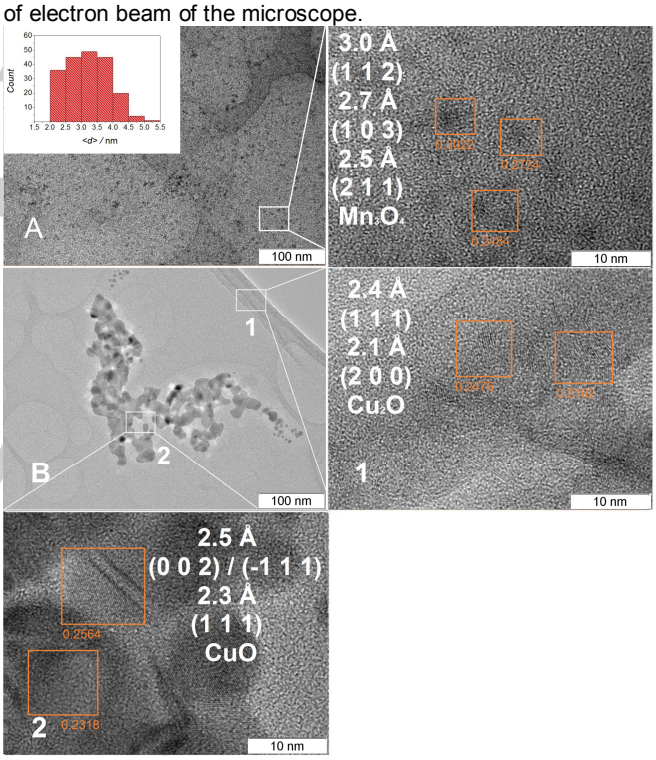

Figure 3. TEM images of freshly prepared Mn/1.25%Starch (A) and Cu/1.25%Starch (B) catalysts. Inserts: Cu2O with morphology of CuOH lamellar crystals (B1), nanoparticles of Cu^{II} oxide (B2). [Cu] = [Mn] = 2×10^{-3} M. [Starch]= 12.5 g L^{-1}.

The photon-correlation light scattering was used to determine hydrodynamic diameter of particles both of starch and of Fe-, Cu-, Co- Mn-containing catalysts in their aqueous solutions (Table 2, Figs. 4, 5, 6). The studies of solutions of not activated and activated starch (1250 mg in 100 mL water) free of metal atoms (the fresh solution of not activated starch, see Fig. 4A;

fresh solution of activated starch and the solution stored for a week, see Figs. 4B, C) revealed that the thermal activation resulted in a decrease in the average particle size from 17 ± 5 to 6 ± 2 nm. The starch particles changed only negligibly in size on storage: 6 ± 2 nm in the fresh solution, 7 ± 3 nm in a week. The scattering intensity of the all starch solutions was no more than 2 % of Io that did not allow us to obtain accurate results of starch particles size. With the catalyst solutions, the scattering intensity was more than 10 %, probably due to the size of colloidal particles and dark colors of the solutions; the results obtained were more accurate (Fig. 5 and 6). The Fe/0.125%Starch catalyst prepared with non-activated starch (fresh, see Fig. 5C; the one in 168 h, see Fig. 5D) was studied to show that the particles did not increase noticeably in size on storage: 14 ± 5 nm against 17 ± 5 nm. The average hydrodynamic diameters of the particles equal to 7 ± 3, 5 ± 2 and 7 ± 2 nm were determined in fresh catalysts Fe/0.125%Starch, Mn/1.25%Starch, Co/1.25%Starch, respectively (Figs. 5A, 6A, 6C). DLS studies showed the particle diameter as large as three times of that obtained by TEM.

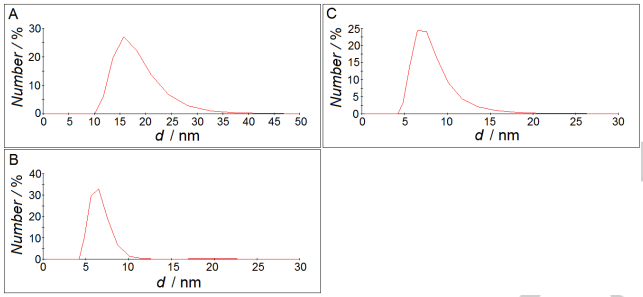

Figure 4. Dynamic light scattering data for not activated starch after 24h (A) and activated starch solutions after 24h (B) and 168h (C) of aging. [Starch]= 12.5 g L-1.

Hence, the data obtained by this method are general information on the hydroxide nucleus and stabilizing starch molecules. On ageing of Fe- and Co-containing catalysts for a week, the particles grew in size: from 7 ± 3 to 64 ± 5 (Fe) and from 5 ± 2 to 62 ± 2 nm (Co). However, while TEM data indicate the constant size of metal oxide crystallites, the observed growth in size occurs due to agglomeration of individual starch particles via formation of hydrogen bonds between the starch molecules.

The results on testing of the catalysts stored for a week argue for the same: the catalyst particles, even though grown in size, keep their activity and selectivity identical to those of the fresh samples. This would be impossible with enlarged starch envelope (the selectivity decreased when more starch was used) or coarsening of the hydroxide particles (the TEM data indicate preservation of the size of metal-containing particles, and the catalysts prepared with not activated starch and containing hydroxide agglomerates are low active). Probably, dissolution of the aged catalyst in the buffer solution results in dispersing of agglomerates of colloidal particles under the action of counter ions, and the catalytic activity and selectivity remains high. The low active Cu-containing catalyst comprises coarse particles (40–140 nm, see Fig. 6D) in agreement with the TEM data.

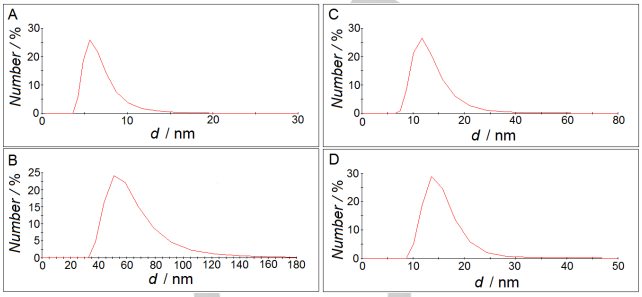

Figure 5. Dynamic light scattering data for Fe/0.125%Starch catalysts: stabilized by activated starch after 24 (A) and 168 h (B) of aging, stabilized by not activate starch after 24 (C) and 168 h (D) of aging. [Fe] = 2×10^{-3} M, [Starch] = 1.25 g L^{-1}.

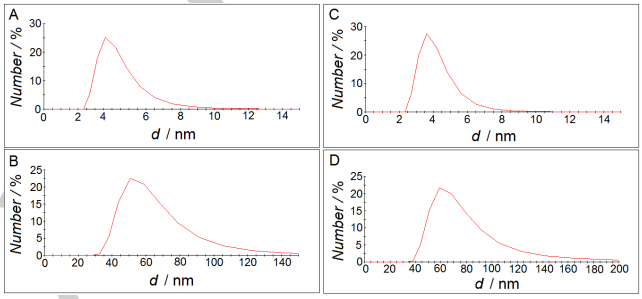

Figure 6. Dynamic light scattering data for catalysts: Co/1.25%Starch after 24 h (A) and 168 h (B) of aging, Mn/1.25%Starch (C), Cu/1.25%Starch 24 h (D). [Co] = [Mn] = [Cu] = 2×10-3 M, [Starch] = 12.5 g L-1.

Physicochemical studies led to conclude about the nucleus/shell type structure of the colloidal particles based on Mn, Fe and Co hydroxides. The primary nanosize particles of hydroxo compounds of the metals (2–3 nm in average size) are nuclei confined in the molecular starch networks. On ageing, the particles of ca. 60 nm in average size are formed owing to the formation of agglomerates containing several hydroxide nuclei isolated from one another and bound through hydrogen bonds of starch molecules. These particles are suspended in the solution, do not precipitate on storage, and are dispersed in the buffer. Therefore, these are rather promising catalysts for stop-flow studies of the kinetics of water oxidation.

Catalyst modeling via molecular mechanics approach

In order to get insights of the structure of colloidal catalyst particles in the solution we used molecular mechanics[32] for modeling the process of binding the Fe^{III} hydroxide by starch molecule. While hydroxide particles bind by starch via formation of hydrogen bonds between glucosidic residues (···C–OH) and surface hydroxyl groups of hydroxide (···Fe–OH), this approach is thought to produce reliable results. The applied AMBER force field allows describing the interaction of large organic polymer molecules (starch in the particular case) in the solution taking into account mainly the contribution of energetics of hydrogen bonds and van der Waals interactions between starch molecules and hydroxide particles[33]. The Periodic Continuum Box conditions and permanent dielectric

constant (ε = 1) allowed us to estimate binding energy of hydroxide particles by starch molecules with allowance for the energy influence of solvent molecules. Application of the molecular mechanics method needs data on the structures of interacting compounds and on electric charges per each atom. Database of the program package HyperChem 8.0 provided data on geometry and the charges per atoms of glucose monomers bound through glycoside bonds in the amylose molecule α(1-4). Molecules of amylose starch in aqueous solutions adopt the structure of the so-called helix formed by hydrogen bonds between the glucose subunits of different coils[34]. We observed the formation of such helix structures (Fig. 7) during the starch molecules optimization using the molecular mechanics model (force field AMBER) in the periodic continuum box. A single coil of the starch helix takes twelve glucose molecules connected by the α(1-4) glycosidic bonds to form a channel with the external diameter of 21.5 Å and the internal one of 10.3 Å. This starch channel has the quite hydrophilic external surface but more hydrophobic internal surface[35].

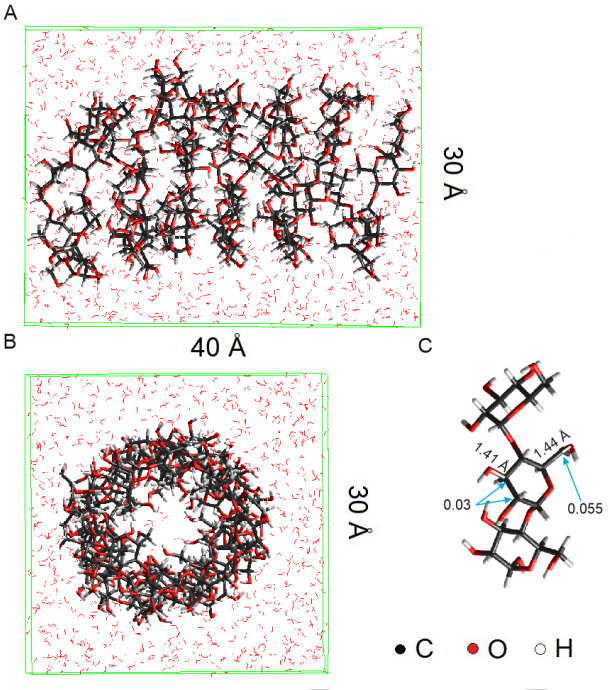

Figure 7. Structure of not activated starch molecule $(C_6H_{12}O_6)_{50}$ established by molecular mechanics method (Force field – AMBER, dielectric constant ε = 1, periodic continuum box 30×30×40 Å, Hyperchem 8.0). Not activated starch $(C_6H_{12}O_6)_{50}$ plus 1189 H_2O. Front view (A) and top view (B) on the starch helix. The effective charges on carbon atoms of C-O-H groups and C-O bond length (C).

Some literature data were used for modeling the iron hydroxide cluster. Zhang and co-authors[27] used centroid molecular dynamics with combined set of force fields[36,37] and additional central force model for water[38] for modeling the process of nucleation of Fe^{III} hydroxide. These simulation results showed that during the early stages of hydrolysis there is occurs the coagulation processes and formation of amorphous primary hydroxide particles (1-2 nm). The further ageing leads to release of the water molecules and formation of FeOOH particles. Our TEM data show that the Fe_2O_3 crystallites are 1.9 nm in average size (Table 2), therefore, we chose the spherical cluster $Fe_{27}O_{27}OH_{27}$ with close diameter (1.2 nm) as a hydroxide particle for our calculations. We optimized the structure of the chosen cluster using semi-empirical PM6 technique (MOPAC2016)[39]. Note that the iron oxo/hydroxide clusters have a complex structure and a wide set of high and low spin states[40] which are not taken into account in the model we used. However, the semi-empirical method which we used for the calculations provides sufficient data on the electron structure and geometry of the chosen Fe^{III} hydroxide geometry (Fig. 8).

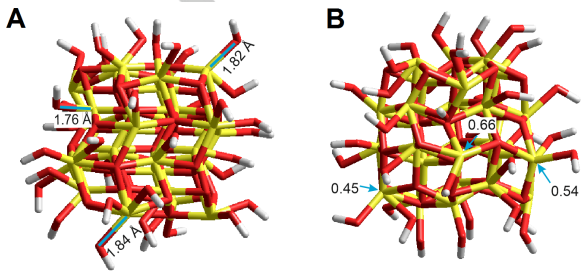

Figure 8. Structure of the Fe-hydroxide ($Fe_{27}O_{27}OH_{27}$) cluster as it was established by the PM6 method (MOPAC2016). A) side view, the length of surface Fe-O bond is shown; B) Top view, the local charges on surface Fe ions are shown.

The hydroxides are moderately hydrophilic compounds, and the hydroxide particles are expected to move towards the position inside the channel of the starch helix. However, incorporation of an hydroxide particle into the internal space of the starch channel is low probable because of small size of the channel (1.03 nm). Hydroxide cluster can also be stabilized on the external surface of the helix. To discriminate against these possibilities, we calculated the stabilization energy for the not activated starch containing 50 glucose monomers ($(C_6H_{10}O_5)_{50}$) and activated starch containing 15 glucose monomers ($(C_6H_{10}O_5)_{15}$). Recall that the polymerization degrees of the chosen starch samples were estimated using the copper ratio[31]. The stabilization energy was calculated by formula:

$$\Delta E_{stabilization} = E_3 - (E_1 + E_2) \quad (6)$$

where E_1 is the total energy of hydrated iron hydroxide cluster ($Fe_{27}O_{27}OH_{27}$ + 1189 H_2O); E_2 is the total energy of hydrated starch molecule ($(C_6H_{10}O_5)_{50}$ + 1189 H_2O); E_3 is the total energy of hydrated hydroxide stabilized with starch molecule ($Fe_{27}O_{27}OH_{27}$ + $(C_6H_{10}O_5)_{50}$ + 1189 H_2O). Despite the fact that the calculation was carried out for the system at 0 K, and the solvation energy changes due to the formation of bonds between the hydroxide cluster and the starch molecule, the results obtained allowed us to compare the value of $\Delta E_{stabilization}$

that made it possible to estimate the probability of the stabilization.

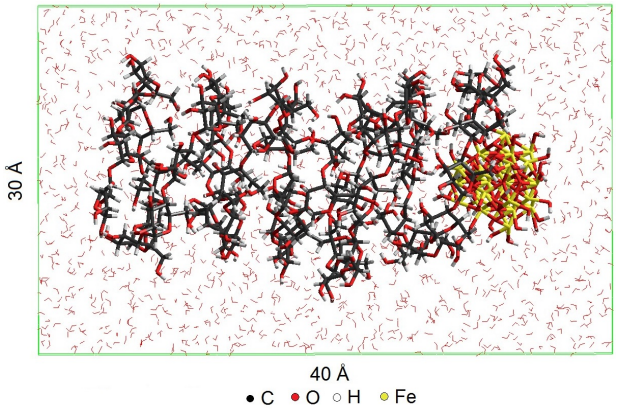

Figure 9. Structure of Fe-hydroxide catalysts stabilized by N.A. starch established by molecular mechanics method (Force field – AMBER, dielectric constant ε = 1, periodic continuum box 30×30×40 Å, Hyperchem 8.0). Not activated starch $(C_6H_{12}O_6)_{50}$ plus $Fe_{27}O_{27}OH_{27}$ and 1189 H_2O.

With not activated starch, binding the hydroxide species to form hydrogen bonds occurs either on the external surface of the starch molecule or at the channel inlet. The most energetic benefit is observed in the latter case ($\Delta E_{stabilization}$ = -27 ± 4 kCal/mol) that indicate the optimal energetics of such a structure. In the former case, $\Delta E_{stabilization}$ is lower (–12 ± 3 kCal/mol). The hydroxide stabilization inside the helix needs it to unfold, but the energy benefit of the stabilization does not compensate its loss due to the helix unfolding ($\Delta E_{stabilization}$ = 5 ± 2 kCal/mol) that makes the process energetically unfavorable. Fig. 9 illustrates the optimized structure of the hydroxide particle at the inlet of the channel of the non-activated starch molecule.

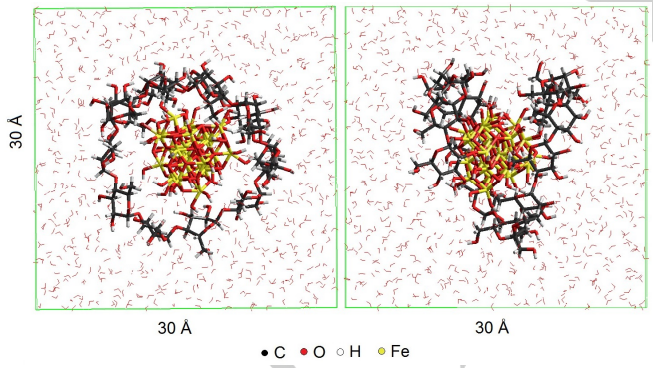

Figure 10. Structure of Fe-hydroxide catalysts stabilized by thermally dextrated starch established by molecular mechanics method (Force field – AMBER, dielectric constant ε = 1, periodic continuum box 30×30×30 Å, Hyperchem 8.0). Thermally dextrated starch $(C_6H_{12}O_6)_{15}$ plus $Fe_{27}O_{27}OH_{27}$ and H_2O.

The calculation on the activated starch containing 15 monomers of glucose $(C_6H_{10}O_5)_{15}$ showed the helix to unfold (due to cleavage of intramolecular hydrogen bonds) and which allow the metal hydroxide particles to draw into the starch shell. A shorter chain and, as a consequence, a lower energy of interaction between helix laps makes it possible to unfold the helix and to produce the core-shell structure. Fig. 10 illustrates the optimized structure of hydroxide $Fe_{27}O_{27}OH_{27}$ bound by dextrated starch. In this case, $\Delta E_{stabilization}$ is as high as –41 ± 4 kCal/mol. Hence, one may expect that the stabilization of the metal hydroxide cluster by molecules of thermo activated starch follows this way to form the core-shall structure. Here, the metal hydroxide particles remain exposed both to the substrate and oxidant molecules, while the external hydrophilic surface of the starch molecule provides good solubility of the catalyst.

The influence of pH, metal nature and catalyst concentration on oxygen yields

Dependence of the oxygen yield on the conditions of water oxidation with the trivalent ruthenium tris-bipyridyl complex was studied in detail in the presence of the most effective catalysts by varying the nature and concentration of the catalytically active metal, pH of the reaction mixture, and the buffer nature

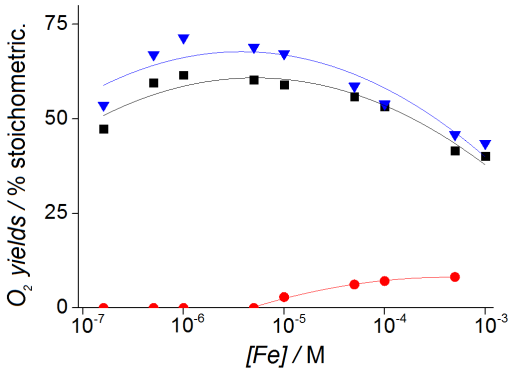

(Figs. 11–14).

Figure 11. The influence of pH and concentration of Fe/0.125%Starch catalyst on the oxygen yields. ▼ – pH 10.0, 0,06 M Borate buffer, ■ – pH 9.2, 0.06 M Borate buffer, ● – pH 7.0, 0.06 M Phosphate buffer, $[Ru(bpy)_3^{3+}]$ = 5×10^{-4} M, [Cat] = $10^{-7}\div10^{-3}$ M, 25 ml, 298 K.

The oxygen yields were determined over a wide range of the catalyst concentrations (10^{-7}–10^{-3} M) at pH 7.0, 9.2, 10.0 of the solution. The phosphate buffer was used to obtain pH 7.0 while the borate buffer for pH 9.2 and 10.0. With all the catalysts (Fe, Mn, Co, Cu), we observed similar bell-like dependences of the oxygen yield on the concentration of the catalytically active metal at all pH under study. The oxygen yields increase with the catalyst concentration to reach their maxima at the oxidant/catalyst ratio of 10–500 and decrease at the further increase in the catalyst concentration. These dependencies can be used for determining relationships between the rates of the formation of oxygen and the products of known side reactions (catalytic and non-catalytic destruction of the oxidant through oxidation of the organic ligand (bipyridyl))[41].

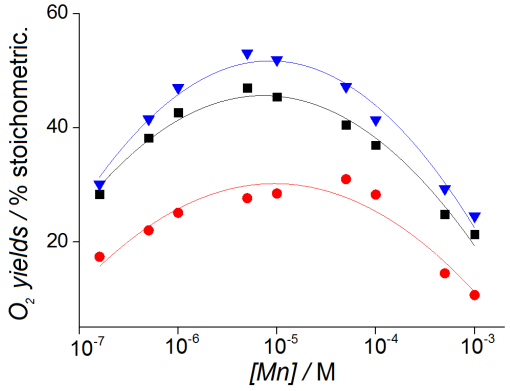

Figure 12. The influence of pH and concentration of Mn/1.25%Starch catalyst on the oxygen yields. ▼– pH 10.0, 0.06 M Borate buffer, ■ – pH 9.2, 0.06 M Borate buffer, ● – pH 7.0, 0.06 M Phosphate buffer, $[Ru(bpy)_3^{3+}]$ = 5×10^{-4} M, [Cat] = $10^{-7}\div10^{-3}$ M, 25 ml, 298 K.

$$(1\text{-}x)Ru(bpy)_3^{3+} + 3x(bpy)_{coord.} + 0.2H_2O \longrightarrow (1\text{-}x)Ru(bpy)_3^{2+} + 0.1CO_2 + 0.4H^+ + \text{tar products} \quad (7)$$

$$Ru(bpy)_3^{3+} + 3(bpy)_{coord} \xrightarrow{cat} Ru(bpy)_3^{2+} + 0.1CO_2 + 0.4H^+ + \text{tar products} \quad (8)$$

A decrease in the oxygen yield results from the non-catalytic destruction (7) at the low catalyst concentration and from the catalytic destruction (8) at the high catalyst concentration: If the catalytic destruction does not occur, the oxygen yield would increase monotonically with the catalyst concentration to reach 100 % in respect of the reaction (3) stoichiometry but this is not the case[40-43]. The typical curves of the oxygen yield on the catalyst concentration in reaction (3) are bell-shaped, the maximal yields of 100 % being never observed even under the most favorable conditions. This is an evidence existence of some common stages and intermediates of the reactions of water oxidation and bipyridyl destruction.

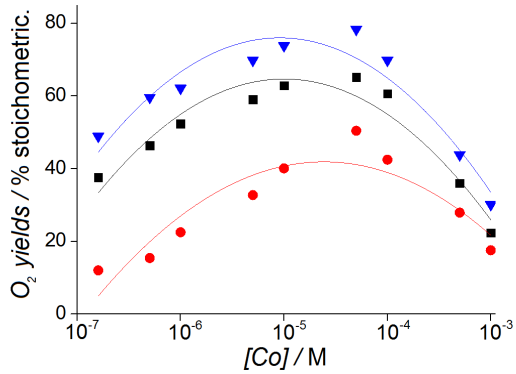

Figure 13. The influence of pH and concentration of Co/1.25%Starch catalyst on the oxygen yields. ▼- pH 10.0, 0.06 M Borate buffer, ■ – pH 9.2, 0.06 M Borate buffer, ● - pH 7.0, 0.06 M Phosphate buffer, $[Ru(bpy)_3^{3+}]$ = 5×10^{-4} M, [Cat] = $10^{-7}\div10^{-3}$ M, 25 ml, 298 K.

The oxygen yields over all the catalysts under study were maximal when the borate buffer at pH 10.0 was used. The maximal oxygen yields were 78 % (TON = 7.8) over Co/1.25%Starch at the catalyst concentration 5×10^{-5} M ($Co/Ru(bpy)_3^{3+}$ = 1/10), 53 % over the Mn-containing catalyst at 5×10^{-6} M ($Mn/Ru(bpy)_3^{3+}$ = 1/100), 72 % over the Fe-containing catalyst (TON = 360) at 1×10^{-6} M ($Fe/Ru(bpy)_3^{3+}$ = 1/500). At decreasing of pH down to 9.2 a decrease in the oxygen yields over all the catalysts (the maximal yields were 65 % for Co, 47 % for Mn, 65 % for Fe) is observed at the same optimal catalyst concentrations. The Cu/1.25%Starch catalyst was least active; it provided the maximal oxygen yield of 28 % at pH 9.2 and copper concentration 1×10^{-5} M ($Cu/Ru(bpy)_3^{3+}$ = 1/50).

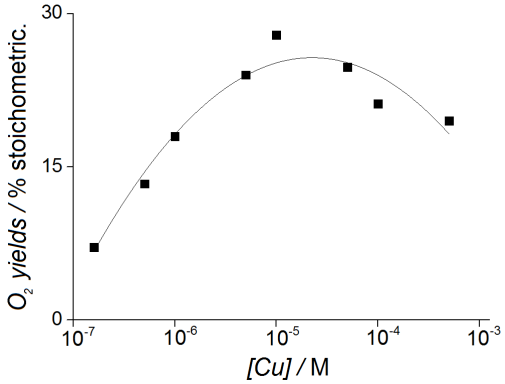

Figure 14. The influence of pH and concentration of Cu/1.25%Starch catalyst on the oxygen yields. pH 9.2 0,06 M Borate buffer, $[Ru(bpy)_3^{3+}]$ = 5×10^{-4} M, [Cat] = $10^{-7}\div10^{-3}$ M, 25 ml, 298 K.

A sharp decrease in the oxygen yield in the presence of the Fe-containing catalyst in the phosphate buffer at pH 7.0 may be accounted for by the formation of insoluble iron phosphate. This assumption is supported by the difference in the oxygen yields over Fe/0.125%Starch at [Fe]= 10^{-6} M in 0.06 M borate and phosphate buffers at identical pH 8.0: The oxygen evolution is inhibited (8 %) in the phosphate buffer but reaches 47 % of the stoichiometric amount in the borate buffer. With the catalyst stabilized by a great quantity of starch, Fe/1.25%Starch, 0.06 M phosphate buffer at pH 7.0 and [Fe]= 10^{-6}–10^{-3} M, the oxygen yield was no more than 9 % of the stoichiometric yield. The TEM studies of the Fe/0.125%Starch catalyst after its interaction with the phosphate buffer revealed the presence of trace of the Fe^{III} phosphate phase and a bulk phase of amorphous Fe_2O_3. One may suppose that iron hydroxide is leached from starch owing to the interaction between phosphate ions and starch molecules. On the other hand, in the presence of the Co-containing catalyst in the buffer free solution at pH 11.0 (obtained by adding 1 M NaOH), the oxygen yield was as low as 24 % and pH decreased to 5.5. One of the reasons for the considerable decrease in the oxygen yield may be degradation of the active catalyst centers under the action of protons generated during the water oxidation. These two facts indicate a lability of starch as the

ligand. Hence, to provide the maximal efficiency of the colloidal catalysts needs the influence of surrounding anions of the buffer medium to be taken into account. Again, the colloidal catalysts, due to the starch lability, are expected to be useful as precursors for anchoring nanosize particles of catalytically active metals onto various supports. Such anchored nanosize catalysts are promising for developing of biomimetic systems for artificial photosynthesis and/or overall water decomposition to molecular hydrogen and oxygen where all the processes (water oxidation to dioxygen, water reduction to dihydrogen and absorption of light quanta followed charge separation) reside on one substrate[44, 45].

Conclusions

Application of dextrated starch as a stabilizer of colloidal hydroxides of transition metals (Fe^{III}, Mn^{III}, Co^{III}) allowed the process of hydroxide ageing to be stopped at the stage of the formation of primary nuclei (2–3 nm) and catalysts for water oxidation to dioxygen, which are stable on storage and under the reaction conditions (pH 7–11) to be prepared. The catalyst preparation conditions (order of the component mixing, temperature of synthesis, starch concentration, pH) are optimized. Physicochemical (TEM, DLS) studies of the catalysts and modeling of their structure by molecular mechanics methods lead to conclude about the core-shell type structure of the colloidal catalyst particles. The catalytically active core of metal hydroxide (2–3 nm) is covered by the molecular starch network (5–7 nm) that makes it stable in aqueous media and prevents the growth of hydroxide particles. Fe-, Mn- and Co-containing catalysts appear to be highly efficient to oxidation of water with one electron oxidant $Ru(bpy)_3^{3+}$. The influence of pH, catalyst concentration and buffer nature on the oxygen yield is studied. The maximal yields are 71, 53 and 78 % over Fe-, Mn- and Co-containing catalysts, respectively, while TON are 7.8, 54 and 360, respectively. The catalyst prepared on the basis of Cu^{II} comprises coarse hydroxide particles (20–40 nm) and appear to be only poorly effective to water oxidation (the maximal yield is 28 % O_2). In addition, some features of catalysts based on nanosize metal hydroxo compounds are in common with the natural oxygen-evolving complex: polynuclear structure and the ability of adsorbing and stabilizing water molecules and intermediates of water oxidation on their surface. Hopefully, the further stop-flow kinetic studies of the reaction mechanism in the presence of starch stabilized colloidal hydroxide catalysts will be useful in establishing the mechanism of action of the natural oxygen evolving complex. In addition, the developed colloidal catalysts can be used as precursors for anchoring nanosize particles of catalytically active metals onto various supports in order to develop biomimetic systems for complete photocatalytic decomposition of water.

Experimental Section

Chemicals and materials

All the solutions were prepared with deionized water obtained using a Milli-Q (Millipore) treatment system. The following reagents were used: $Ru(OH)Cl_3$ (pure), $CoCl_2$ (analytically pure), $KMnO_4$ (analytically pure), $Cu(Ac)_2$ (analytically pure), $Fe(NO_3)_3$ (analytically pure), HCl (high pure), H_2SO_4 (high pure), HNO_3 (high pure), $HClO_4$ (high pure), NaOH (Panreac), LiOH (high pure), $NaClO_4$ (high pure), acetone (high pure), ethanol (commercial, 96%), $KHCO_3$ (analytically pure), H_2O_2(high pure), $(NH_4)_2CO_3$ (analytically pure), water soluble starch for iodimetry (analytically pure), HBO_3 (high grade), $NaHC_4H_4O_6$ (high grade), $KNaC_4H_4O_6$ (analytically pure), CuSO4 (analytically pure), $(NH4)_2Fe_2(SO_4)_6$ (analytically pure), Na_2HPO_4 (analytically pure), NaH_2PO_4 (analytically pure).

Catalyst preparation

The catalysts were prepared by hydrolysis of an appropriate metal hydroxide precursor in the presence of dissolved starch[25, 26]. Water soluble starch for iodimetry (amylase) was thermally pre-treated (dextracted) in air. Metal-containing precursors of the catalysts were aqueous solutions (in 5 mL of water): 84 mg $Mn(bpy)Cl_3$ (synthesized by the method given elsewhere[46]), 40 mg $Fe(NO_3)_3$, 24 mg $Cu(Ac)_2$. The Co-containing catalyst was prepared by dissolving 35 mg of $Co(NH_3)_2(CO_3)_2$ (synthesized by the method given elsewhere[47]) in 5 mL of 0.25 M HNO_3 for 2 hours until complete removal of carbon dioxide. The quantities of the precursors were chosen to provide the final metal concentration of 2×10^{-3} M in the catalyst solutions. Samples of 125– 1250 mg of thermo activated starch (to reach the concentrations of 0.125–1.25 wt %, respectively) were dissolved in 45 mL of water at 350 K under continuous stirring with a magnetic stirrer. After that the solution of a metal-containing precursor was added portion wise (50 µL) alternately with an alkali solution (100–150 µL of 1M NaOH or 1M LiOH for TEM characterization of the catalysts) at constant temperature (350 K) under vigorous stirring. pH of the solution was controlled using an ANION 4100 instrument (Russia) to keep it close to 11.0. The resulting solution was left under stirring for 10 min at 350 °C, cooled to room temperature in argon, diluted with water to 100 mL, and stored in argon at 286 K. Three different procedures were used for preparing Co-containing catalysts: (1) the solution of Co-precursor (5 ml of 2×10^{-2} M complex $Co(NH_3)_2(CO_3)_2$ dissolved in 2.5×10^{-1} M HNO_3) was added to 45 ml of an alkali solution (pH 11.0) of starch (12.5 g L^{-1}) at 350 K; (2) the solution of 1 M NaOH (~ 1.5 ml) was added to the 45 ml of the Co-precursor (2×10^{-3} M) solution with starch (12.5 g L^{-1}) to reach pH 11.0 at 350 K; (3) the dropwise addition of small portions (50 µL) of the Co-precursor (5 ml of 2×10^{-2} M complex $Co(NH_3)_2(CO_3)_2$ dissolved in 2.5×10^{-1} M HNO_3) followed by addition of alkali solution (portions of 1 M NaOH ~ 100-150 µL to maintain constant pH 11.0) to the 45 ml of starch solution (12.5 g L^{-1}) at 350 K.

Physicochemical characterization of catalysts

The average number of monomers in starch molecules was determined based on the copper ratio using the reaction of the aldehyde group of starch and Fehling's solution[31]. High resolution transmission electron spectroscopic technique (HRTEM) was used for characterization of the catalysts structures prepared with 1 M LiOH instead of NaOH and containing 2×10^{-3} M of Mn, Co and Cu stabilized with 1.25% of starch, as well as those containing 2×10-3 M of Fe stabilized with 0.125% of starch, both fresh samples and the solutions aged for seven days being studied. An electron microscope JEM 2010 (JEOL, Japan) operated at 200 kV accelerating voltage and limit lattice resolution 0.14 nm was used. The images were acquired using CCD matrix of Soft Imaging System (Germany). The instrument was equipped with an energy

dispersive detector of X-ray characteristic radiation (EDX) XFlash (Bruker, Germany) and a semiconductor Si-detector with 130 eV energy resolution. Specimens to be studied with the electron microscope were prepared by supporting the sample particles onto perforated carbon substrates mounted on copper ones using an ultrasonic disperser in order to provide the uniform particle distribution through the substrate surface. The sample was immersed within ethanol covering the ultrasonic disperser, ethanol evaporated, and the sample particles deposited onto the copper grid.

Catalysts (Mn/1.25%Starch, Co/1.25%Starch, Cu/1.25%Starch и Fe/0.125%Starch) prepared with 1M NaOH were characterized using photon correlation spectroscopy (Malvern Nanosizer NS, UK). A starch containing sample (1250 mg of starch was dissolved in 48 mL of water; pH 11.0 was provided by adding 2 mL of 1M NaOH) was used as the reference. There were 3 to 6 iterations of each measurement of both fresh samples and samples stored for a week.

Modeling of catalysts via molecular mechanics

The semi-empirical quantum chemical technique PM6 with MOPAC2016 software[38] was used for optimizing structure of the hydroxide cluster ($Fe_{27}O_{27}OH_{27}$). Program package HyperChem 8.0 was used to estimate the energetics of stabilization of hydroxide with starch molecule and to find an optimal conformation of colloidal catalyst nanoparticles. Molecular mechanics calculations were performed in the AMBER force field[33] using the Periodic Continuum Boxes 30×30×40 Å (1189 water molecules) for a starch molecule with the polymerization number equal to 50, and 30×30×30 Å (892 water molecules) for a starch molecule with the polymerization number equal to 15 at invariable dielectric constant ε=1.

Testing of catalysts at water oxidation by $Ru(bpy)_3^{3+}$

Catalysts were tested using the reaction of water oxidation by complex $Ru(bpy)_3(ClO_4)_3$. The complex was prepared by oxidizing $Ru(bpy)_3(ClO_4)_2$ with PbO_2[48]. The $Ru(bpy)_3(ClO_4)_2$ was synthesized from $Ru(OH)Cl_3$ using the known procedure[49]. The target product, $Ru(bpy)_3(ClO_4)_3$, comprised no more than 5 % of the initial two-valent complex according to the UV-Vis data obtained with a Agilent Cary 60 (USA) spectrometer at λ=452 nm (ε=14 000). Water was oxidized in a 25 mL polyethylene reactor mounted in a jacketed glass vessel; the temperature was kept at 298 K using a TEPMEX VT-8-02 thermostat. A Clark electrode (764080 Dissolved Oxygen Probe, Germany) connected to an oxygen meter (HI 2004 edge, Germany) was used for detecting the yields of oxygen in the solution. The reactor with the catalyst solution (10^{-7}÷10^{-3} M) in 24 mL buffer solution (0.06 M borate buffer at pH 9.2, 10.0 or 0.06 M phosphate buffer at pH 7.00) was blown through with argon for ca. 15 min until the oxygen meter showed zero oxygen content. After blowing was stopped, 1 mL of aqueous solution of 24 mg $Ru(bpy)_3^{3+}$ was added, the reactor rapidly and hermetically sealed, and stirring turned on. The oxygen concentration in the solution was monitored with the oxygen meter. The oxygen yield was calculated as percentage in respect of the oxidant used with allowance for the reaction stoichiometry. The turnover number (TON) was calculated by formula:

$$TON = [O_2] / [M] \quad (9)$$

where $[O_2]$ is the concentration of evolved oxygen, mol L^{-1}; [M] is concentration of metal ions of the catalyst in the solution, mol L^{-1}.

Acknowledgements

We acknowledge gratefully E.Yu. Gerasimov from the Boreskov Institute of Catalysis SB RAS for the TEM characterization. We also acknowledge gratefully V.L. Kuznetsov from the Boreskov Institute of Catalysis SB RAS for the assistance in the molecular mechanics modeling. This work was partially supported by the Russian Foundation for Basic Research (project 15-29-01275) and by budget projects (0303-2016-0012 for BIC SB RAS and 0356-2016-0503 for ICCT SB RAS).

Keywords: water splitting • one-electron oxidants • transition metal hydroxides • catalytic activity • oxygen evolution reaction

[1] N. Cox, D.A. Pantazis, F. Neese, W. Lubitz, *Interface Focus* **2015**, 5(3), 1-10.
[2] K.I. Zamaraev, V.N. Parmon, *Catal. Rew.* **1980**, 2, 261-324.
[3] K. Sanderson, *Nature* **2008**, 452, 400-402.
[4] G.W. Brudvig, *Phil. Trans. R. Soc. B.* **2008**, 363, 1211-1219.
[5] T. Zidki, L. Zhang, V. Shafirovich, S.V. Lymar, *J. Am. Chem. Soc.* ***2012*** 134(35), 14275-14278.
[6] S.A. Bonke, A.M. Bond, L. Spiccia, A.N. Simonov, *J. of Am. Chem. Soc.* **2016**, 138, 16095-16104.
[7] H. Osgood, S.V. Devaguptapu, H. Xu, J. Cho, G. Wu, *Nano Tod.* **2016**, 11(5), 601-625.
[8] B.M. Hunter, H.B. Gray, A.M. Müller, *Chem. Rev.* **2016,** 116(22), 14120-14136.
[9] M.M. Najafpour, S.I. Allakhverdiev, *J. Photochem. Photobiol. B: Biol.* **2015**, 152, 127-132.
[10] P. Du, R. Eisenberg, *En. Env. Sci.* **2012**, 5(3), 6012-6021.
[11] E.A. Paoli, F. Masini, R. Frydendal, I.E.L. Stephens, I. Chorkendorff, *Chem. Sci.* **2015**, 6(1), 190-196.
[12] I.D. Young, M. Ibrahim, R. Chatterjee, S. Gul, F.D. Fuller, S. Koroidov, A.S. Brewster, R. Tran, R. Alonso-Mori, T. Kroll, T. Michels-Clark, H. Laksmono, R.G. Sierra, C.A. Stan, R. Hussein, M. Zhang, L. Douthit, M. Kubin, C. De Lichtenberg, L. Vo Pham, H. Nilsson, M.H. Cheah, D. Shevela, C. Saracini, M.A. Bean, I. Seuffert, D. Sokaras, T.-C. Weng, E. Pastor, C. Weninger, T. Fransson, L. Lassalle, P. Bräuer, P. Aller, P.T. Docker, B. Andi, A.M. Orville, J.M. Glownia, S. Nelson, M. Sikorski, D. Zhu, M.S. Hunter, T.J. Lane, A. Aquila, J.E. Koglin, J. Robinson, M. Liang, S. Boutet, A.Y. Lyubimov, M. Uervirojnangkoorn, N.W. Moriarty, D. Liebschner, P.V. Afonine, D.G. Waterman, G. Evans, P. Wernet, H. Dobbek, W.I. Weis, A.T. Brunger, P.H. Zwart, P.D. Adams, A. Zouni, J. Messinger, U. Bergmann, N.K. Sauter, J. Kern, V.K. Yachandra, J. Yano, *Nature* **2016**, 540(7633), 453-457.
[13] A. Singh, M. Fekete, T. Gengenbach, A.N. Simonov, R.K. Hocking, S.L.Y. Chang, M. Rothmann, S. Powar, D. Fu, Z. Hu, Q. Wu, Y.-B. Cheng, U. Bach, L. Spiccia, *ChemSusChem* **2015**, 8(24), 4266-4274.
[14] G.L. Elizarova, G.M. Zhidomirov, V.N. Parmon, *Catal. Tod.* **2000**, 58, 71-88.
[15] A.S. Chikunov, O.P. Taran, A.A. Shubin, I.L. Zil'berberg, V.N. Parmon, *Kin. Catal.* **2018**, 59(1), 23–47.
[16] D.J. Vinyard, G.W. Brudvig, *Ann. Rew. of Phys. Chem.* **2017,** 68, 101-116.
[17] P.E.M. Siegbahn, *J. of Photochem. and Photobiol. B: Biology* **2011,** 104(1-2), 94-99.
[18] P.E.M. Siegbahn, *Proc. Nat. Ac. Sci. USA*. **2017,** 114(19), 4966-4968.
[19] P. Peerakiatkhajohn, J.-H. Yun, S. Wang, L. Wang, *Adv. Mat.* **2016,** 6405-6410.
[20] H. Zhou, R. Yan, D. Zhang, T. Fan, *Chem. - A Eur. J.* **2016**, 22(29), 9870-9885.

[21] R. Pokhrel, M.K. Goetz, S.E. Shaner, X. Wu, S.S. Stahl, *J. Am. Chem. Soc.* **2015,** 137(26), 8384-8387.

[22] M. Suga, F. Akita, M. Sugahara, M. Kubo, Y. Nakajima, T. Nakane, K. Yamashita, Y. Umena, M. Nakabayashi, T. Yamane, T. Nakano, M. Suzuki, T. Masuda, S. Inoue, T. Kimura, T. Nomura, S. Yonekura, L.-J. Yu, T. Sakamoto, T. Motomura, J.-H. Chen, Y. Kato, T. Noguchi, K. Tono, Y. Joti, T. Kameshima, T. Hatsui, E. Nango, R. Tanaka, H. Naitow, Y. Matsuura, A. Yamashita, M. Yamamoto, O. Nureki, M. Yabashi, T. Ishikawa, S. Iwata, J.-R. Shen, *Nature* **2017,** 543(7643), 131-135.

[23] W. Schneider, Comm. *Inorg. Chem.: A J. Crit. Disc. Curr. Liter.* **1984**, 3(4), 205-223.

[24] M.M. Najafpour, M.Z. Ghobadi, B. Haghighi, T. Tomo, J.-R. Shen, S.I. Allakhverdiev, *Biochim. Biophys. Acta Bioenerg.* **2015**, 1847(2), 294-306.

[25] G.L. Elizarova, L.G. Matvinenko, O.P. Taran, V.N. Parmon, V.N. Kolomiichuk, *Kin. Catal.* **1992,** 33(4), 723-729

[26] G.L. Elizarova, L.G. Matvienko, O.P. Pestunova, V.N. Parmon, *Kin. Catal.* **1994**, 35(3), 329-333

[27] H. Zhang, G.A. Waychunas, J.F. Banfield, *J. Phys. Chem. B.* **2015,** 119(33), 10630-10642.

[28] C.M. Flynn Jr., Chem. Rev. **1984**, 84(1), 31-41.

[29] A.L. Rose, M.W. Bligh, R.N. Collins, T.D. Waite, Langmuir. **2014**, 30(12), 3548-3556.

[30] J. Scheck, B. Wu, M. Drechsler, R. Rosenberg, A. E. S. Van Driessche, T. M. Stawski, D. Gebauer, *J. Phys. Chem. Lett.* **2016**, 7(16), 3123-3130.

[31] H. Fehling, Die quantitative Bestimmung von Zucker und Stärkmehl mittelst Kupfervitriol. Justus Liebigs Annalen der Chemie **1849**, 72(1), 106-113.

[32] U. Burkert, N.L. Allinger, Molecular Mechanics, ACS Monograph 177, ACS, Washington, D.C., **1982**

[33] C.I. Bayly, K.M. Merz, D.M. *J. Am. Chem. Soc.* **1995,** 117(19), 5179-5197.

[34] A.C. Eliasson, W. Wahlgren, *Food Sci., Technol. Nutrition.* **2004**, 441-460.

[35] S. Immel, F.W. Lichtenthaler, The Hydrophobic Topographies of Amylose and its Blue Iodine Complex. Starch/Staerke **2000**, 52(1), 1-8

[36] N.H. De Leeuw, T.G. Cooper, *Geochim. Cosmochim. Acta* **2007,** 71, 1655−1673.

[37] D. Spagnoli, D.J. Cooke, S. Kerisit, S.C. *J. Mater. Chem.* **2006**, 16, 1997−2006.

[38] F.H. Stillinger, A. Rahman, *J. Chem. Phys.* **1978**, 68, 666−670.

[39] Stewart, *J.J.P. J. Mol. Model.* **2007,** 13: 1173.

[40] G.L. Gutsev, K.G. Belay, L.G. Gutsev, B.R. Ramachandran, *J. Comput. Chem.* 2016, 2527-2536.

[41] O.P. Pestunova, G.L. Elizarova, V.N. Parmon, *Kin. Catal.* **2000,** 41(3), 340-348.

[42] P.K. Ghosh, B.S. Brunschwig, M. Chou, C. Creuts, N. Sutin, *J. Amer. Chem. Soc.* **1984**, 106(17), 4772-4783.

[43] A.P. Moravskii, N.K. Khanonov, A.V. Khramov, V.Ya. Shafirovich, A.E. Shilov, *Soviet J. of Chem. Phys.* **1984**, 3(11), 1584-1590

[44] M.B. Hunter, H.B. Gray, A.M. Müller, *Chem. Rev.* **2016,** 116(22), 14120-14136

[45] Y. Yan, B.Y. Xia, B. Zhao, X. Wang, *J. Mat. Chem. A.* **2016**, 4(45), 17587-17603.

[46] H.A. Goodwin, R.N. Sylva, *Austr. J. Chem.* **1965**, 11, 1743-1749.

[47] M. Mori, M. Shibata, E.B. Kyuno, *Nippon kagaku zassi* **1956,** 77(9), 1434-1437.

[48] R.E. DeSimone, R.S. Drago, *J. of Am. Chem. Soc.* **1970**, 92(8), 2343-2352.

[49] C.F. Liu, *Inorg. Chem.* **1964**, 3(8), 1085-1087.

Entry for the Table of Contents

FULL PAPER

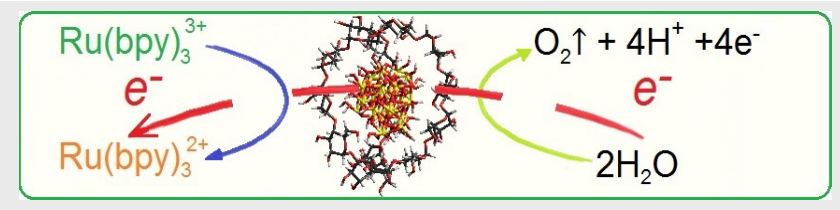

Stabilization of primary nuclei products of Fe^{III}, Mn^{III}, Co^{III} salts hydrolysis using dextrated starch result in formation of an effective catalysts of water oxidation reaction at weakly basic pH (7.0 - 10.0) with high selectivity (72, 53 and 78 %) in presence of one – electron oxidant $Ru(bpy)_3^{3+}$.

A.S. Chikunov, O.P. Taran, I.A. Pyshnaya, V.N. Parmon

Page No. – Page No.

Colloidal Fe^{III}, Mn^{III}, Co^{III} and Cu^{II} hydroxides stabilized by starch as catalysts of water oxidation reaction with one electron oxidant $Ru(bpy)_3^{3+}$